Chapter 3

Fiber-laser-based Sensor Network with Self-Healing Function

3.1 Self-Healing Ring Architecture

In recent years, the ring topology based on electrical add-drop multiplexers for the SDH/SONET has been widely applied in a fiber network where high reliability and low cost are required [1]. In this section, we present a novel FBG sensor network with a self-healing function to increase the reliability. The self-healing function is constructed by using the ring topology. A 1x2 switch in the ring topology is used to check the breakpoint and 2x2 switches are used to enhance the sensing capacity in the sensor network. Such a simple self-healing function for the ring topology can support real-time monitoring and reveal the sudden breakpoint of the fiber link. Furthermore, we use a linear-cavity fiber laser scheme for our proposed sensor system. This sensor network can avoid the reduction of the SNR because of the low-power broadband source together with its ASE noise. The benefits of our proposed fiber-laser-based sensor system can facilitate reliable sensor network for a large-scale smart structure.

3.1.1 Architecture Description

Figure 3.1 shows the proposed configuration of the self-healing FBG sensor

network. The FBG sensor system consists of the sensing FBG network and a central office (CO) providing the light source and discriminating the signals from the sensing network. The light source in this system is a linear-cavity fiber laser that comprises a fiber loop mirror, the sensing FBG (λ_1, λ_2,… or λ_M) simultaneously acting as another cavity mirror, a polarization controller (PC), a tunable bandpass filter (TF), and a section of erbium-doped fiber (EDF) pumped by a 980nm laser diode (LD). The ring architecture for this sensing network is composed of the sensing FBGs ($\lambda_1 \sim \lambda_M$), a piece of single mode fiber (SMF), and a 2x2 switch (SW). *N* groups of such a ring sub-network (Sensing Region 1 ~ Sensing Region N) can be cascaded one by one for constructing a large-scale ring architecture. The 2x2 switch in each sub-network is controlled by a TDM signal to enhance the capacity for multipoint sensing. For example, the dashed line in Fig. 3.2 schematically indicates the situation when Sensing Region 2 is selected by using the TDM signal. Because of this ring topology incorporated with the TDM technology, the proposed system can support a large number of sensor elements. Furthermore, for such a large-scale sensing network, we consider the self-healing function for the ring architecture by controlling the 1x2 switch. Such a self-healing architecture can offer survival function under link failure by reconfiguring the fiber network. Fig. 3.3 schematically shows a situation when the fiber link fails in Sensing Region N-1. When the 1x2 switch is in state (a), we lose the sensing signal from FBG(λ_1) in Region N-1. Nevertheless, the 1x2 switch can be modified to state (b) to reconfigure the sensing signal from FBG(λ_1) in Region N-1. The drawback of this self-healing function for the sensing network protection is that all the switches in the network induce extra loss and further reduce the SNR in the system. In order to enhance the SNR, we

adopt the linear-cavity fiber laser configuration. The capability of this fiber-laser-based sensor system is implemented by tuning a tunable bandpass filter located within the laser cavity for interrogating the Bragg wavelengths of all sensing FBGs. The Bragg wavelength shifts induced by the qusi-static strain or temperature drift on the sensing FBGs can be measured by discriminating the lasing wavelength shifts of the system.

3.1.2 Experimental Results and Discussion

Figure 3.4 shows the experimental setup for our proposed FBG sensor network. We examined three sub-networks in the self-healing ring architecture. Each sub-network included ten sensing FBGs λ_i (i=1, 2, …,10). The Bragg wavelengths of the sensing FBGs from FBG λ_1 to FBG λ_{10} sequentially were 1538.45, 1540.22, 1542.86, 1544.3, 1546.79, 1548.47, 1550.48, 1552.43, 1554.5, and 1556.51 nm. All the peak reflectivities of the FBGs were approximately 99% and their average 3-dB bandwidth were 0.2 nm. In the central office, the lasing wavelength of the linear-cavity fiber laser was determined by these sensing FBGs in conjunction with the tunable bandpass filter (TF). The average 3-dB bandwidth of this TF is 0.37 nm. A 980nm laser diode with 140mW output power pumped the EDF via a 980/1550 nm wavelength division multiplexer coupler (CW). In this linear-cavity fiber laser scheme, the coupling ratio of the 2x2 coupler (C1) for the fiber loop mirror was 30:70. The lasing light emerging from this 2x2 coupler arrived in a photo detector (PD). This signal from the photo detector finally was fed into a microprocessor for discrimination of the lasing wavelength. With sufficient gain, the system lases once the transmitted wavelength of the filter equals the wavelength reflected from the sensing grating. Thus, the lasing wavelength of

the system can be used to accurately measure the strain perturbation imposed on the FBGs. The filter was tuned by using a controller to select the transmitted wavelength over a working range from 1530nm to 1560nm. Hence the tunable transmitted wavelength of the filter tracked the ten wavelengths of the sensing FBGs λ_i (i=1, 2, …,10). The output spectra of the linear-cavity fiber laser at different lasing wavelengths are shown in Fig. 3.5. The average lasing peak power was 9.98mW leading to the SNR for the sensing network over 52 dB. When the link failed at Region 2, the FBGs λ_m (m=6, 7, 8, 9, 10) lost their sensing information whenever Sensing Region 2 was selected by using a TDM signal, as shown in Fig. 3.6. Nevertheless, state (b) of the 1x2 switch can be modified to reconfigure the fiber link for FBGs λ_m (m=6, 7, 8, 9, 10) that lost the sensing information, as shown in Fig. 3.7. Consequently, the self-healing ring architecture can regenerate the sensing signal.

We further concentrate our experiment on the performance of the entire sensing network. Three important issues regarding the practical limitations on our proposed sensor structure are discussed: (i) The lasing power limits the scale of the sensing network. Although the switches and tunable filter facilitate the multiplexeing of FBG sensors, they also increase cavity losses and degrade the lasing power. In our experiment, the insertion loss of each 1x2 switch and 2x2 switch were below 1dB; likewise the insertion loss of the filter is 3.42dB in 1530-1560nm wavelength region. In addition, the reflectivity of the fiber loop mirror is 84%. To estimate the network scale, we assume that the total splicing loss and insertion loss in each sub-network (including ten FBGs) is 2.3 dB. With a 25dB-gain of our EDF amplifier, the proposed self-healing structure could support seventeen sub-networks. (ii) Even though the linear-cavity fiber

laser with high SNR could support large-scale sensing network, too many sub-networks will lead to poor response time of the system. The operating time on each FBG in the ring architecture are limited by both the TDM signal and the sweeping time of the filter. From 1530 nm to 1560 nm the maximum tuning speed of our filter was 920 ms; and the switching time of each switch was 1 ms. Therefore, under the device restrictions of our laboratory, the variation of the quasi-static strain imposed on each FBGs cannot be over 0.18 Hz for this sensor system with three sub-networks. The system response time can be improved by reducing the scale of sensing network, by reducing the number of FBGs in each sub-network for smaller sweaping time of tunable filter, and basically by using a faster tunable filter. (iii) The stability of the lasing wavelength and the crosstalk induced by the adjacent FBGs also limit the number of FBG sensors. To avoid such degradation, a feedback-controlled circuitry [2] can be used in the system. For example, we chose 1.44 nm as the minimum wavelength spacing between the sensing FBGs in our experiment. This wavelength spacing indicates that the maximum strain imposed on each FBG has to be smaller than 598 $\mu\varepsilon$ [3] and this quantity should be accurately controlled by the feedback circuitry. According to the above three issues, the optimal self-healing sensor network can be designed by considering the maximum measured strain, the acceptable operating time, and the scale of the ring architecture.

In summary, this section presents a novel self-healing sensor network based on a linear-cavity fiber laser scheme. The sensing network is arranged on the basis of ring architecture. In this paper, we demonstrate a 10 point FBG sensor based on our proposed configuration and examine its network survivability. Because of the intense lasing power from the linear-cavity fiber laser, the SNR

for the sensor network can be over 52dB. Furthermore, the self-healing function considered in our system can reconfigure the fiber link when a breakpoint suddenly occurs in the sensing network. The experimental results show that the proposed system can facilitate highly reliable sensing network for a large-scale and multipoint smart structure. We also discuss three practical limitations of this proposed sensor system.

3.2 Hybrid Star-Ring Architecture

Recently, the modified star-ring architecture has been proposed for subcarrier multiplexed passive optical networks [4]. In this section, we present a hybrid star-ring architecture for FBG sensor systems with a self-healing function to increase the reliability of the sensing network. The hybrid star-ring architecture consists of a star network on the upper level and a series of concatenated ring subnets on the lower level. The ring subnets with self-healing capabilities overcome the weakness in reliability of the star network. Such a self-healing function can be performed at remove notes (RNs) by using optical switches to reconfigure the ring subnets if any link fails. However, the switches in the network introduce extra loss and further reduce the SNR in the system. To solve this problem, we use a linear-cavity fiber laser scheme for our proposed sensor network because the laser has intense output power, high SNR, and ability to be incorporated with fiber communication systems. The sensing FBGs in our proposed system are used simultaneously as the feedback elements of the fiber laser. The benefits of the fiber laser scheme in conjunction with the hybrid star-ring architecture can facilitate highly reliable large-scale sensing in

a smart structure.

3.2.1 Architecture Description

Figure 3.8 shows the proposed configuration of a hybrid star-ring architecture for a FBG sensor system. The FBG sensor system consists of the sensing FBG network and a CO providing the light source and discriminating the signals from the sensor network. In the sensor network, the light source are distributed to the RNs via the upper level star network, and then are further delivered to each FBG sensor through the lower level ring subnets. Every ring subnet is connected by a 2x2 optical switch. The function of RN is to properly transfer signals between the CO and lower level ring subnet, and to perform self-healing function if link failure occurs in the lower level ring subnets. As shown in Fig. 3.9, each RN comprises two 1x2 optical switch (OS) and a 1x2 optical coupler (C1). The states of the optical switches are normally set as shown in Fig. 3.10. The CO signal is properly forwarded to the RN1. If the corresponding link in the lower level ring subnets is broken, the control circuit will reconfigure the RN function as Fig. 3.11 such that the CO signal is forwarded to the RN1 and RN2. When the 2x2 optical switch is at bar state as shown in Fig. 3.11 (a), the FBGs (S_{13} and S_{14}) lose their sensing signals. However, the state of the 2x2 optical switch at cross state as shown in Fig. 3.11 (b) can be modified to reconfigure the signal of the FBGs (S_{13} and S_{14}). The drawback of this hybrid star-ring architecture for FBG sensor system is that the switches in the network introduce extra loss and further reduce the SNR of the system. In order to enhance the SNR, we adopt a linear-cavity fiber laser configuration. The sensing FBGs in our proposed sensor network are also used as the cavity mirrors of the fiber laser. The proposed system can result in a highly reliable sensor network for a multipoint smart structure.

3.2.2 Experimental Results and Discussion

Figure 3.12 shows the experimental setup for our proposed FBG sensor network. The center office in this system comprised a tunable bandpass filter (TF), a 1x2 optical switch, and a section of erbium-doped fiber pumped by a 980nm laser diode (LD), and a fiber loop mirror with a polarization controller (PC) and a 2x2 optical coupler (C2) as a cavity mirror. The lower level ring subnets for this sensing network was composed of the sensing FBGs (S1~S10) and a 2x2 optical switch (SW). The insertion loss of each 1x2 optical switch and 2x2 optical switch were below 1dB. Each of the sensing FBGs (S1~S10) acted as another cavity mirror of the linear-cavity fiber laser. The Bragg wavelengths of the sensing FBGs from S1 to S10 sequentially were 1538.52, 1540.14, 1542.78, 1544.25, 1546.62, 1548.33, 1550.28, 1552.32, 1554.36, and 1556.34 nm. All the peak reflectivities of the FBGs were approximately 99% and their average 3-dB bandwidth were 0.2 nm. In the central office, the lasing wavelength of the linear-cavity fiber laser was determined by these sensing FBGs and the tunable bandpass filter (TF). The average 3-dB bandwidth of this TF was 0.37 nm. The average insertion loss of the filter was 3.42dB in 1530-1560nm wavelength region. A 980nm laser diode with 120mW output power pumped the Er-fiber via a 980/1550 nm WDM coupler (CW). In this linear-cavity fiber laser scheme, the coupling ratio of the 2x2 optical coupler (C2) for the fiber loop mirror was 30:70. In addition, the PC is arranged for the reflectivity of this fiber loop mirror. Hence it is unnecessary for us to adjust the PC for each grating sensor or if a fault occurs in the sensing network. The lasing light emerging from the C2 arrived in a photo detector (PD). This signal from the PD finally was fed into a microprocessor for discrimination of the

lasing wavelength. With sufficient gain, the system lases once the transmitted wavelength of the filter equals the wavelength reflected from the sensing grating. Thus, the lasing wavelength of the system can be used to accurately measure the strain perturbation imposed on the FBGs. The filter was tuned by using a controller to select the transmitted wavelength over a working range from 1530nm to 1560nm. Hence the tunable transmitted wavelength of the filter tracked the ten wavelengths of the sensing FBGs (S1~S10). When the link failed, the FBGs Sm (m=4, 5, 8, 9, 10) lost their sensing information whenever CO was selected the RN1, as shown in Fig. 3.13. Nevertheless, the OS can be modified to reconfigure the fiber link for FBGs Sm (m=4, 5, 8, 9, 10) that lost the sensing information, as shown in Fig. 3.14. The average lasing peak power was 7.68 dBm leading to the SNR for the sensing network over 48 dB. Consequently, the self-healing ring architecture can regenerate the sensing signal.

In the experiment we concentrated our study on how to achieve the star-ring architecture for a FBG sensor system. Thus we only used an optical spectra analyzer (OSA) to measure the lasing wavelength without considering the electronic signal processing. Under this condition, the filter controlled by a stepper motor provided a minimum resolvable wavelength shift of 0.1 nm corresponding to a minimum resolution 83 $\mu\varepsilon$ for the strain [3]. From 1530 nm to 1560 nm the maximum tuning speed of the filter (TB45B from JDS Uniphase Co.) used in our experiment was 920 ms. Therefore, under the device restrictions of our laboratory, the scanning rate is approximately 1 Hz from 1530 nm to 1560 nm. In addition, the switching time of each switch was 1 ms. If two breakpoints occur as shown in Fig. 3.12, the reconfiguration time to

address all FBGs in the sensing network is at least 1841 ms (=920×2+1 ms). Because the interrogation method relies on the tunable filter, the system is more suitable for static or low frequency dynamic strain measurement. This limitation of response time can be improved by reducing the scale of sensing network and basically by using a faster tunable filter. For example, the resolution of the system in Ref. [5] was 60 μ ε for static strain, which was determined by the OSA resolution of 0.07 nm. Dynamic stain frequency is limited less than 5 Hz because of the data processing speed of the system. Such a limitation can be further improved by using suitable electronic signal processing. In Ref. [3] the Fabry-Perot filter via a 16 bit digital-to-analog converter provides a minimum resolvable wavelength shift of approximately 0.8 pm. The Fabry-Perot filter can be scanned at rates ＞300 Hz.

Finally, the proposed sensor scheme is capable of supporting 20 WDM channels with 2 nm per channel. In this case, the range of the measurement for each sensing FBG has to be smaller than [-830, 830] μ ε . However, a partially reflecting fracture of the fiber could result in redundant lasing light, which was examined in our experiment. Because such a redundant signal is weak, we can reduce the pump power to avoid the lasing due to the reflection from a partially reflecting fracture of a fiber. Therefore, the pump power should be determined according to the tradeoff between the sensing scale and the environment that may leads to many fractures. Alternatively, a feedback-controlled circuitry [2] can be adopted to clarify whether the lasing light is a correct sensing signal. Moreover, because of our proposal star-ring architecture, we can reconfigure the sensing branch even if the system lases off fracture.

In conclusion, this section presents a hybrid star-ring architecture for a FBG sensor system. We demonstrate a 10-point FBG sensor based on our proposed configuration

and examine its network survivability. Because of the intense lasing power from the linear-cavity fiber laser, the SNR for the sensor network can be over 48dB. Furthermore, the self-healing function considered in our system can reconfigure the fiber link when a breakpoint suddenly occurs in the sensing network. The experimental results show that the proposed system can facilitate highly reliable sensing network for a large-scale and multipoint smart structure.

3.3 Star-Bus-Ring Architecture

Recently, a high-capacity WDM network based on a self-healing star-bus-ring architecture has been proposed [6]. In this section, we present a self-healing star-bus-ring architecture for increasing the reliability and capacity of FBG sensors. The star-bus-ring architecture consists of star subnets on the upper level, several bus subnets on the middle level, and many ring subnets on the lower level. We design remote nodes using simple optical switches to check the breakpoint and reconfiguring the star-bus-ring architecture if a link fails. However, the switches in the network introduce extra loss and further reduce the SNR of the system. To solve this problem, we use a fiber laser scheme for our proposed sensor network because a laser can provide an intense output power and a high SNR [2]. A self-healing sensor network based on a linear-cavity fiber laser scheme is proposed. The proposed system can enhance the survivability of the FBG sensor system against environmental accidents. It is good for health monitoring of structures such as tunnels, dams, bridges, and buildings because many FBG sensors may be embedded in these structures.

3.3.1 Architecture Description

Figure 3.15 shows the proposed configuration of a star-bus-ring architecture for FBG sensors. The star-bus-ring architecture consists of an FBG sensor network and a central office providing the light source and discriminating sensing signals from the sensor network. The sensor network has a star subnet on the upper level to serve as an infrastructure for the network, several bus networks on the middle level to enhance the capacity, and many ring subnets on the lower level to serve as FBG sensors. The star subnet connects many RNs to the CO. The bus subnet connects two neighboring RNs. Light form the light source is distributed to the RNs via the upper-level star network, and then is further delivered to each FBG sensor through the middle-level bus subnets and lower-level ring subnets. The function of an RN is to properly transfer signals between the CO and middle-level bus subnets, and to perform a self-healing function if link failure occurs in the lower-level network. As shown in Fig. 3.16, each RN comprises three 1x2 optical switches. Many ring subnets are attached to bus subnets via 2x2 optical switches. The ring architecture of this sensor network is composed of FBG sensors (λ_1~λ_{10}) with different wavelengths and a 2x2 optical switch as shown in Fig. 3.17. The 2x2 switch in each ring subnet can be controlled by the TDM signal to enhance the capacity of the WDM-FBG sensor system. For example, the dashed lines in Fig. 3.17(a) and Fig. 3.17(b) schematically indicate the situation when Sensing Region 1 and Region 2 are selected using the TDM signal. Because of this bus topology incorporated with TDM technology, the proposed system can support a large number of sensor elements. Furthermore, for such a large-scale sensor network, we consider the self-healing function of the bus subnets by controlling the RNs. Such a self-healing architecture can offer survival functions under link failure by

reconfiguring the sensor network. Figure 3.18 schematically shows a situation when a fiber link fails in the bus subnets. In this case, the sensing signals lost on Region 4. However, RN3 can be modified to retransmit the sensing signals on Region 4. If the corresponding link in the upper-level star subnets is broken, the control circuit will reconfigure the RN function as shown in Fig. 3.19, such that RN5 can be modified to retransmit the signals of Region 6.

The drawback of this self-healing function for sensing network protection is that all the switches in the network induce extra loss and further reduce the SNR of the system. In order to enhance the SNR, we adopt a linear-cavity fiber laser configuration. The capability of this FBG sensor system is implemented by tuning a tunable band-pass filter located within the laser cavity for interrogating the Bragg wavelengths of all FBG sensors. The Bragg wavelength shifts induced by the strain or temperature drift in the FBG sensors can be measured by discriminating the lasing wavelength shifts of the system. The proposed system can result in a highly reliable sensor network for a multipoint smart structure.

3.3.2 Experimental Results and Discussion

Figure 3.20 shows the experimental setup for our proposed FBG sensor network. We examine two ring subnets in the star-bus-ring architecture. The central office (CO) in this system comprises a tunable band-pass filter (TF), a 1x2 optical switch (OS), and an erbium-doped fiber (EDF) pumped by a 980 nm laser diode, and a fiber loop mirror with a polarization controller (PC) and a 2x2 optical coupler (C) as a cavity mirror. The lower-level ring subnet for this sensor network is composed of FBG sensors (λ1~λ10) and a 2x2 optical switch (SW). The insertion losses of the 1x2 optical switch and 2x2 optical switch are

below 1 dB. Each of the FBG sensors acts as another cavity mirror of the linear-cavity fiber laser. The Bragg wavelengths of the FBG sensors from λ1 to λ10 are respectively 1538.46, 1540.08, 1542.78, 1544.52, 1546.62, 1548.42, 1550.34, 1552.44, 1554.42, and 1556.34 nm. All the peak reflectivities of the FBGs are approximately 99% and their average 3 dB bandwidth is about 0.2 nm. In the central office, the lasing wavelength of the linear-cavity fiber laser is determined by these FBG sensors and the tunable band-pass filter (TF). The average 3 dB bandwidth of this TF is 0.37 nm. The average insertion loss of the filter is 3.7 dB in the 1530-1560 nm wavelength region. The 14 m EDF is pumped using a 980 nm laser diode with a 140 mW output power via a 980/1550 nm WDM coupler (WDM). In this fiber laser scheme, the coupling ratio of the 2x2 optical coupler (C) for the fiber loop mirror is 30:70. In addition, the polarization controller is arranged for the reflectivity of this fiber loop mirror. Hence it is unnecessary for us to adjust the polarization controller for each FBG sensor or if a fault occurs in the sensor network. The lasing light emerging from the 2x2 coupler arrives at a photo detector (PD). This signal from the PD is finally fed into a microprocessor for discrimination of lasing wavelength. With sufficient gain, the system lases once the transmitted wavelength of the filter equals the reflected wavelength of the FBG sensor. Thus, the lasing wavelength of the system can be used to accurately measure the strain or temperature imposed on the FBG sensors. The filter is tuned using a controller to select the transmitted wavelength over a working range from 1530 nm to 1560 nm. Hence the tunable transmitted wavelength of the filter tracks the ten wavelengths of the FBG sensors (λ1~λ10). The dashed line in Fig. 3.21 schematically indicates the situation when Region 7 is selected. The output spectra of the linear-cavity fiber laser at different lasing wavelengths are shown

in Fig. 3.22. The SNR for the sensor network is more than 50 dB. When the link failed at Region 8 as shown in Fig. 3.23, the FBG λm (m=6, 7, 8, 9, and 10) lost their sensing information when the CO selected RN6 as shown in Fig. 3.24. However, when link failure occurred, RN7 was modified to reconfigure the fiber link for FBG λm (m=6, 7, 8, 9, and 10). The lost sensing information can be retransmitted in link reconstruction, as shown in Fig. 3.25. Consequently, our proposed self-healing function can reconstruct the sensor network and enhance capacity.

In summary, we present a star-bus-ring architecture for FBG sensors. The self-healing function is constructed using the remote node. The remote node in the star-bus-ring architecture is used for checking the breakpoint and reconfiguring the star-bus-ring architecture. Moreover, 2x2 switches are used to enhance the sensing capacity of the WDM-FBG sensor system. We have demonstrated two ring subnets based on our proposed configuration and examine their network survivability. Because of the intense lasing power from the linear-cavity fiber laser, the SNR of the sensor network can be more than 50 dB. The experimental results show that the proposed system can facilitate a highly reliable sensing network for a large-scale and multipoint smart structure. Finally, we compare the three proposed architectures as shown in Table 3.1.

References

[1] R. Ramaswami and K. N. Sivarajan, “Optical Networks: A Practical Perspective,” San Francisco, Morgan Kaufmann Publishers Inc., 1998.

[2] Y. Yu, L. Lui, H. Tam, and W. Chung, “Fiber-laser-based wavelength-division multiplexed fiber Bragg grating sensor system,” *IEEE*

Photonics Technology Letters, vol. 13, pp. 702-704, 2001.

[3] A. D. Kersey, M. A. Davis, H. J. Partrick, M. Leblance, K. P. Koo, C. G. Askins, M. A. Putnam, and E. J. Friebele, "Fiber grating sensors," *J. of Lightwave Technology*, vol. 15, pp. 1442-1463, 1997.

[4] W. P. Lin, M. S. Kao, S. Chi, "The modified star-ring architecture for high-capacity subcarrier multiplexed passive optical networks," *J. of Lightwave Technology*, vol. 19, pp. 32-39, 2001.

[5] S. Kim, J. Kwon, S. Kim, and B. Lee, "Multiplexed strain sensor using fiber grating-tuned fiber laser with a semiconductor optical amplifier," *IEEE Photonics Technology Letters*, vol. 13, pp. 350-351, 2001.

[6] W. P. Lin, M. S. Kao, and S. Chi, "A DWDM/SCM self-healing architecture for broad-band subscriber networks," *Journal of Lightwave Technology*, vol. 21, pp. 319-328, 2003.

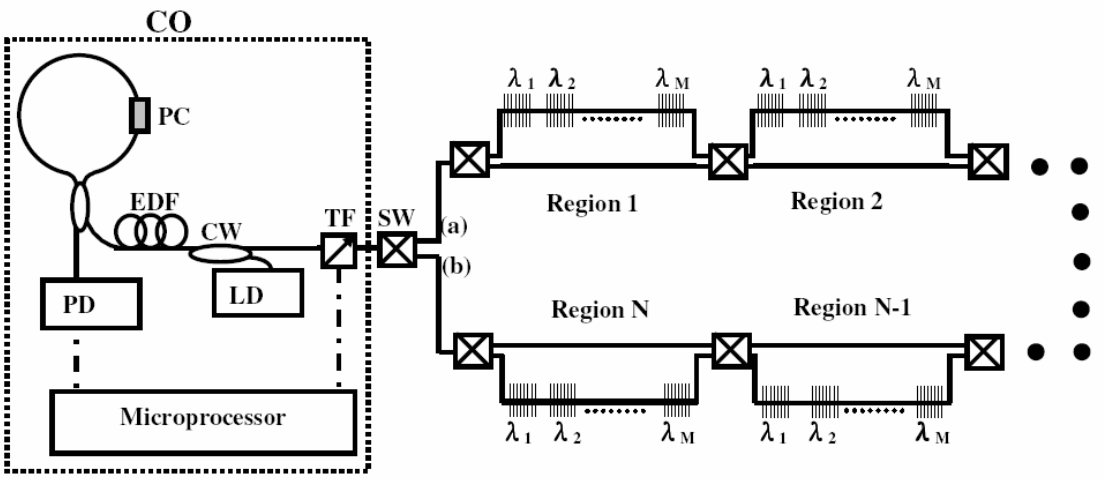

Fig. 3.1 Schematic diagram of the proposed self-healing sensor network based on a linear-cavity fiber laser scheme (PC: polarization controller, TF: tunable bandpass filter, EDF: erbium-doped fiber, LD: 980nm laser diode, λ_i: FBG, C1: 2x2 coupler, SW: switch, CW: WDM coupler, CO: center office, PD: photo detector).

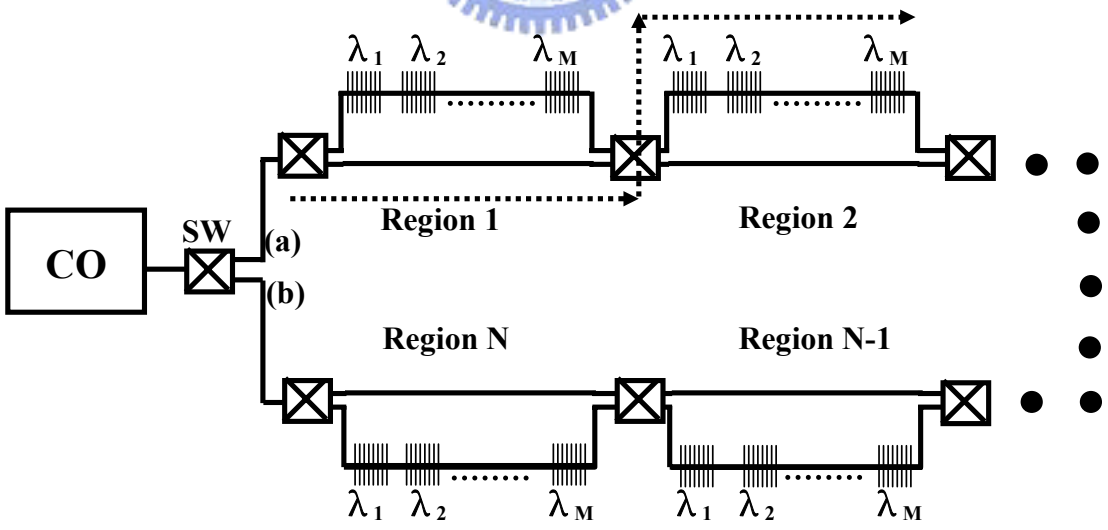

Fig. 3.2 Schematic situation (indicated by the dashed line) when Sensing Region 2 is selected by using a TDM signal.

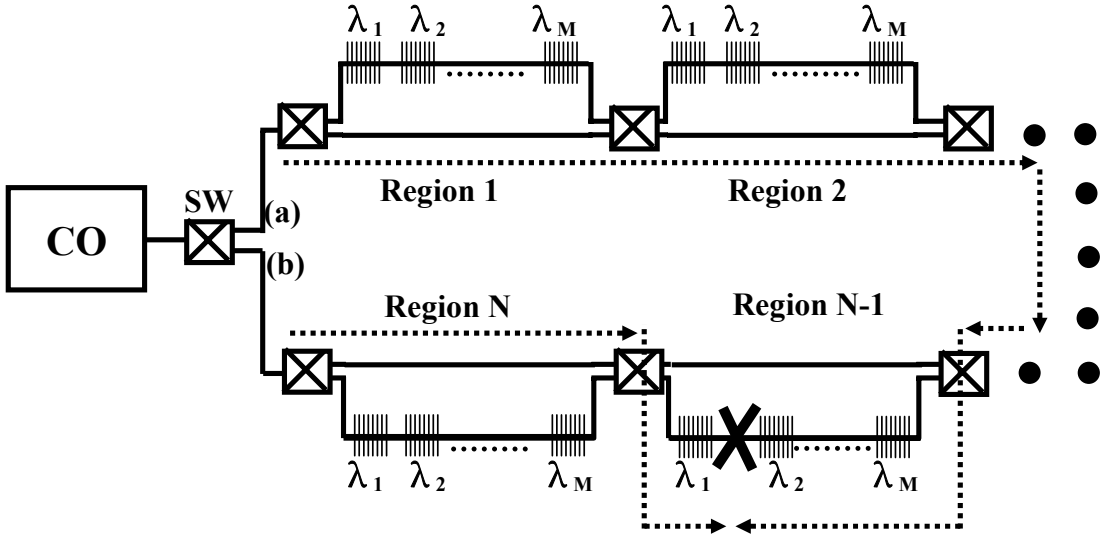

Fig. 3.3 Schematic situation when a breakpoint occurs and the fiber link fails in Sensing Region N-1.

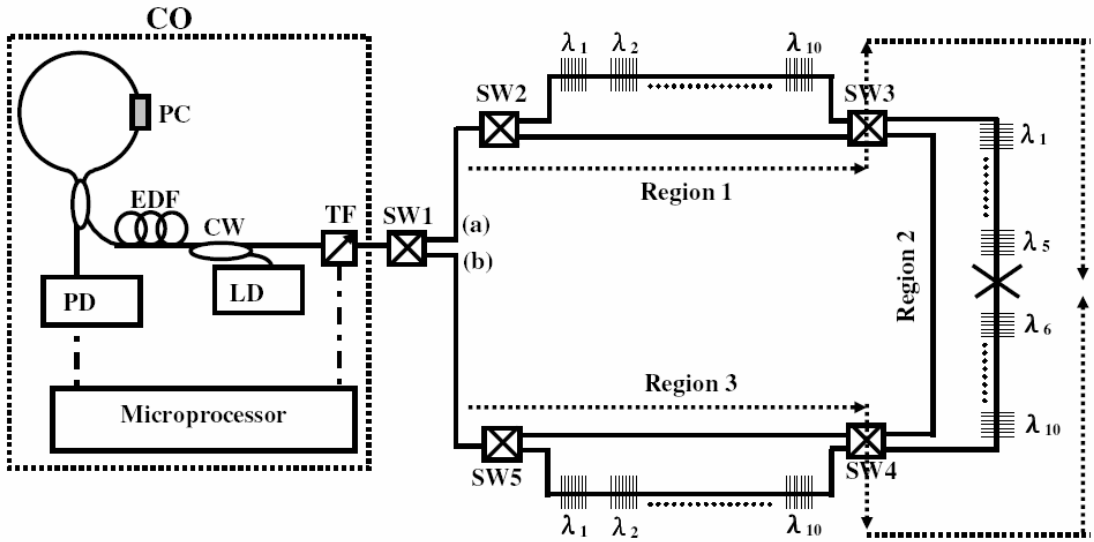

Fig. 3.4 Experimental setup for the proposed FBG sensor network. We examine three sub-networks in the self-healing ring architecture. Each sub-network includes ten sensing FBGs λ_i (i=1, 2, …,10).

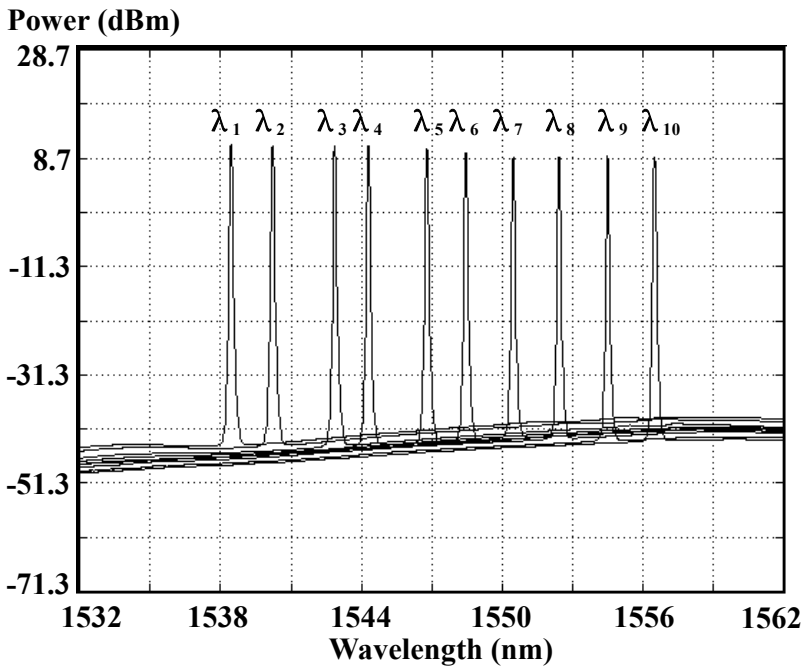

Fig. 3.5 Output spectra of the linear-cavity fiber laser at different lasing wavelengths.

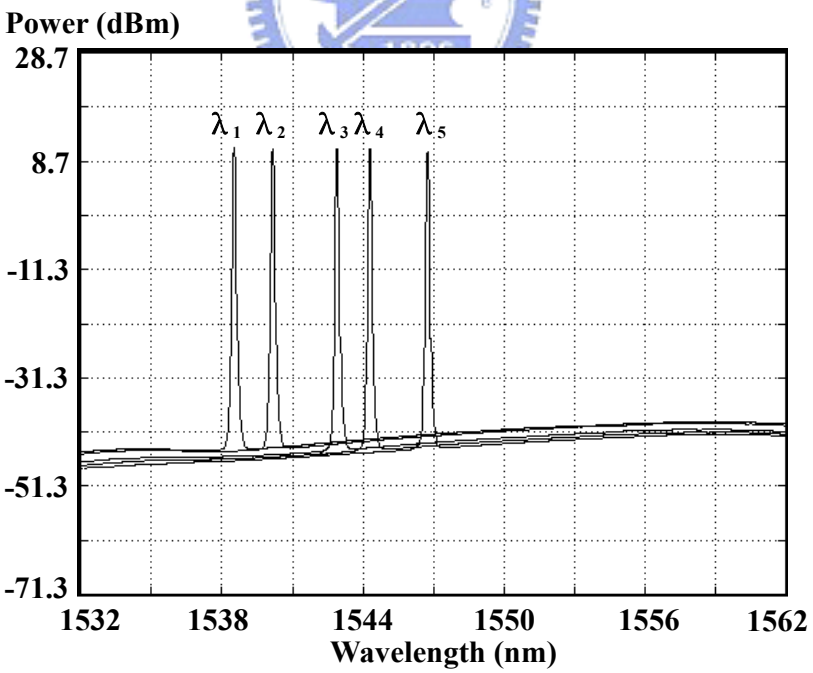

Fig. 3.6 When the link fails in Region 2, the FBGs λ_m (m=6, 7, 8, 9, 10) loses their sensing information whenever Sensing Region 2 is selected by using a TDM signal.

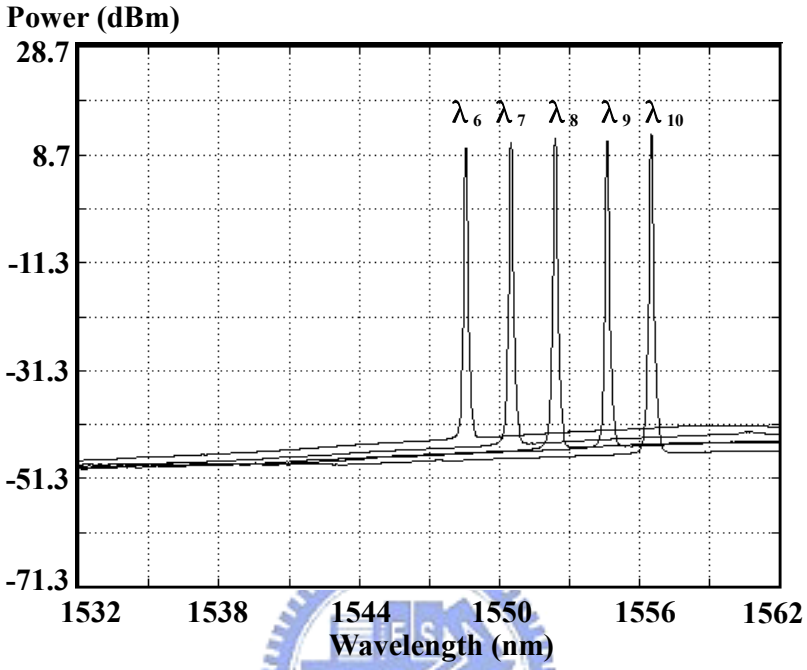

Fig. 3.7 State (b) of the 1x2 switch can be modified to reconfigure the fiber link for FBGs λ_m (m=6, 7, 8, 9, 10) that lost the sensing information. The self-healing ring architecture can regenerate the sensing signals from FBGs λ_m (m=6, 7, 8, 9, 10).

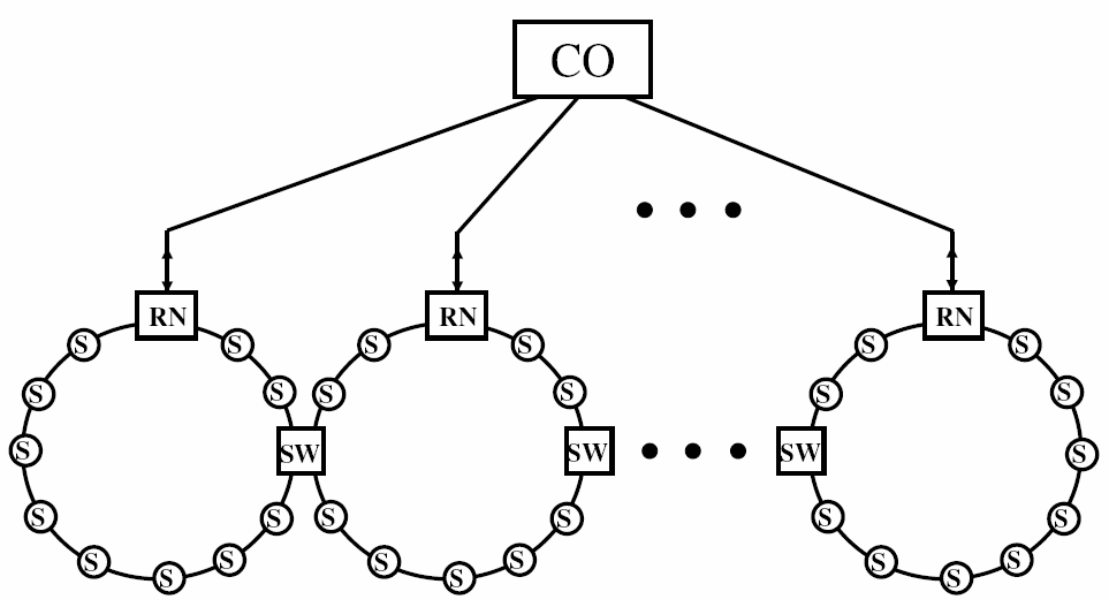

Fig. 3.8 Schematic diagram of a hybrid star-ring architecture for FBG sensor system (CO: center office, RN: remove node, SW: 2x2 optical switch, S: fiber Bragg grating).

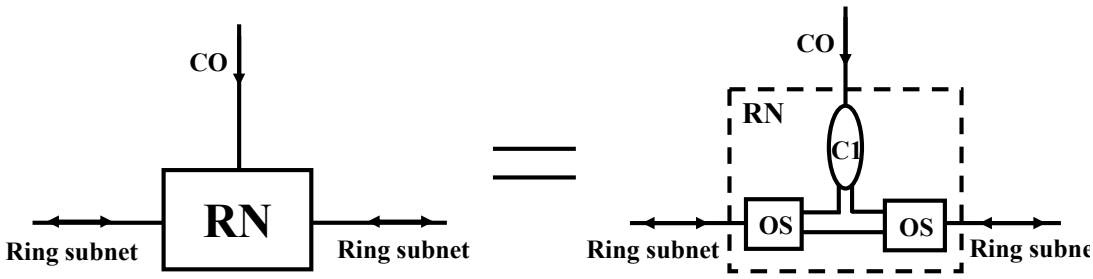

Fig. 3.9 Schematic diagram of a remove node (OS: 1x2 optical switch, C1: 1x2 coupler).

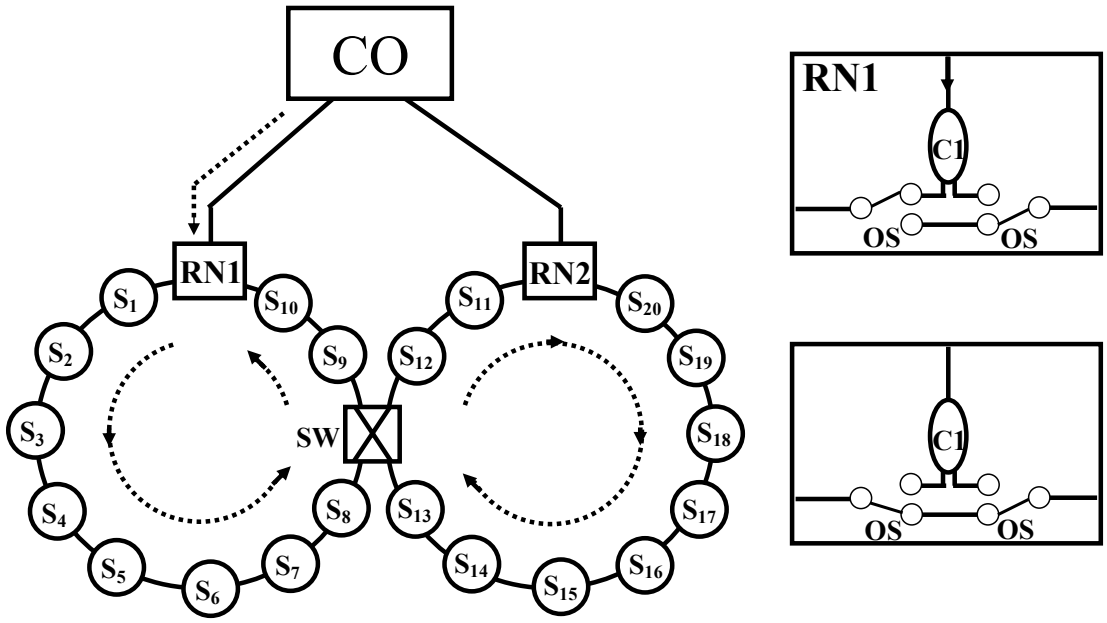

Fig. 3.10 Schematic diagram (indicated by the dashed line) when the optical switchs states are normally set.

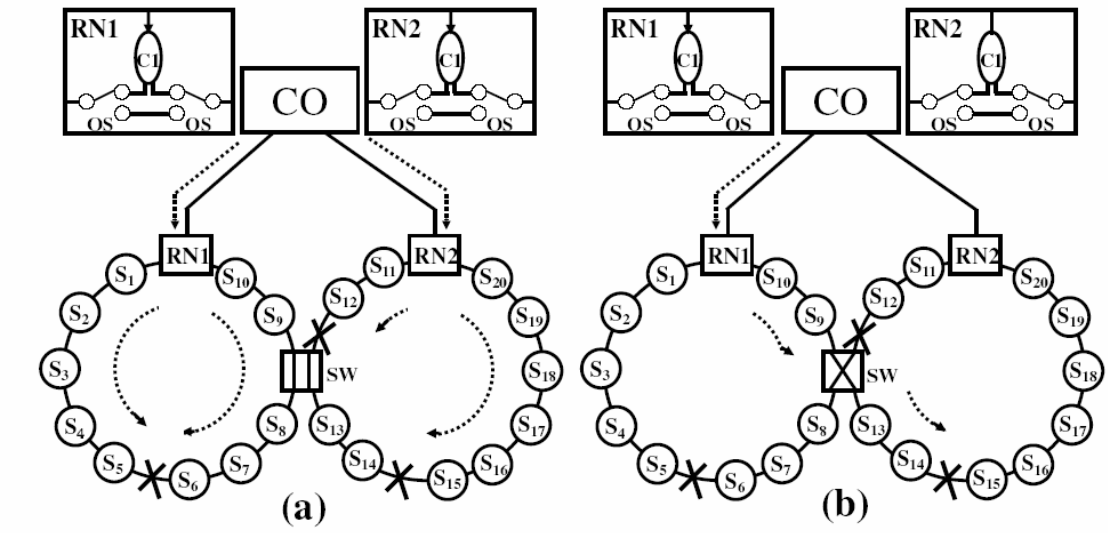

Fig. 3.11 Schematic diagram when three breakpoints occur.

(a) When the SW in the Bar state.

(b) When the SW in the cross state.

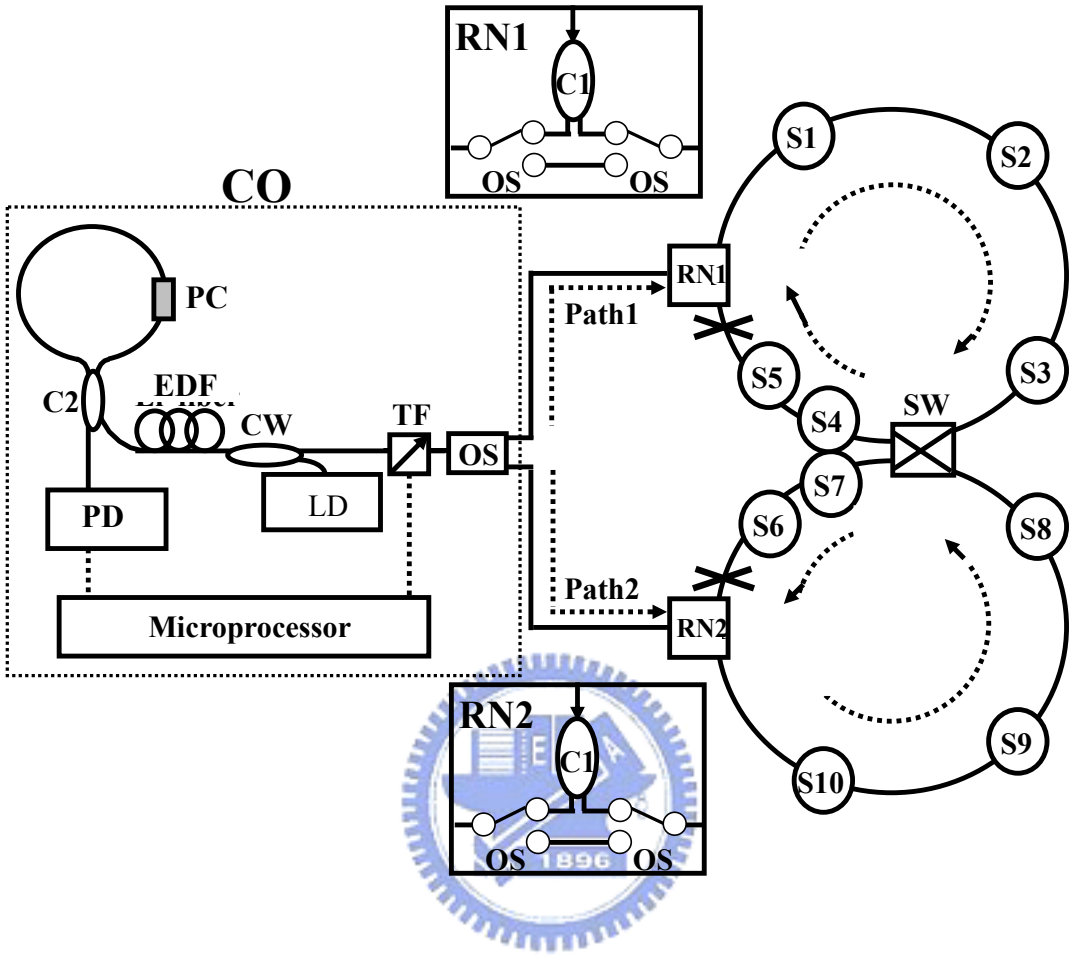

Fig. 3.12 Experimental setup for the proposed FBG sensor network. We examine the case of two breakpoints occur (PC: polarization controller, TF: tunable bandpass filter, Er-fiber: erbium-doped fiber, LD: 980nm laser diode, Sm: FBG, C2: 2x2 coupler, CW: WDM coupler, PD: photo detector).

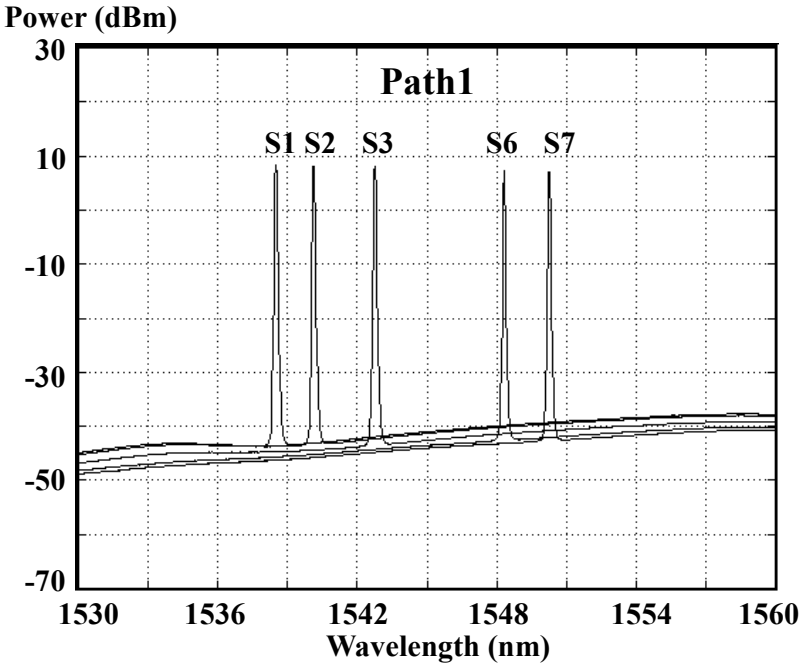

Fig. 3.13 When the link fails, the FBGs Sm (m=4, 5, 8, 9, 10) loses their sensing information.

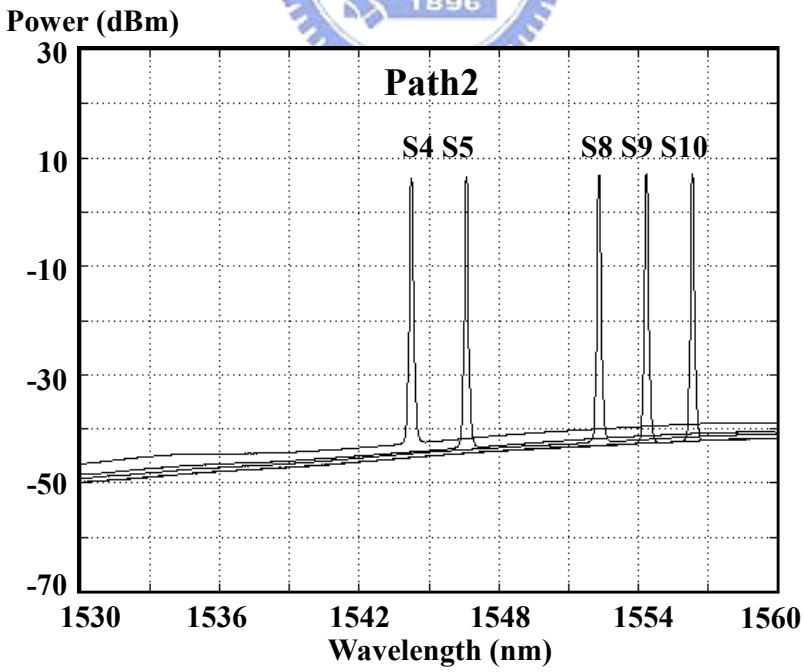

Fig. 3.14 The OS can be modified to reconfigure the fiber link for FBGs Sm (m=4, 5, 8, 9, 10) that lost the sensing information.

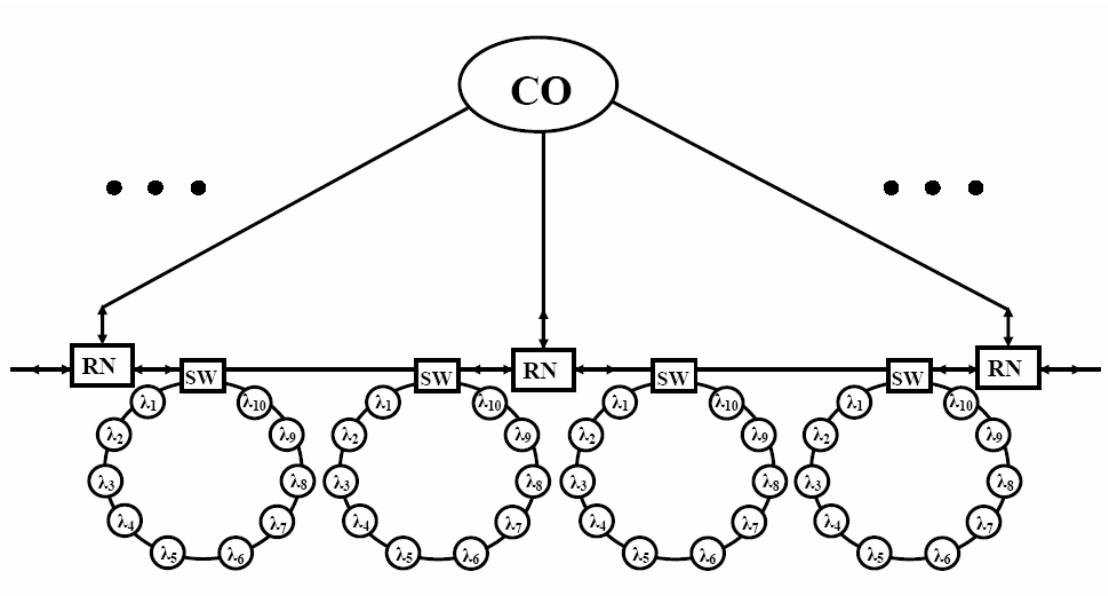

Fig. 3.15 Schematic diagram of star-bus-ring architecture for FBG sensors (CO: central office, RN: remote node, SW: 2x2 optical switch, λ_i: fiber Bragg grating).

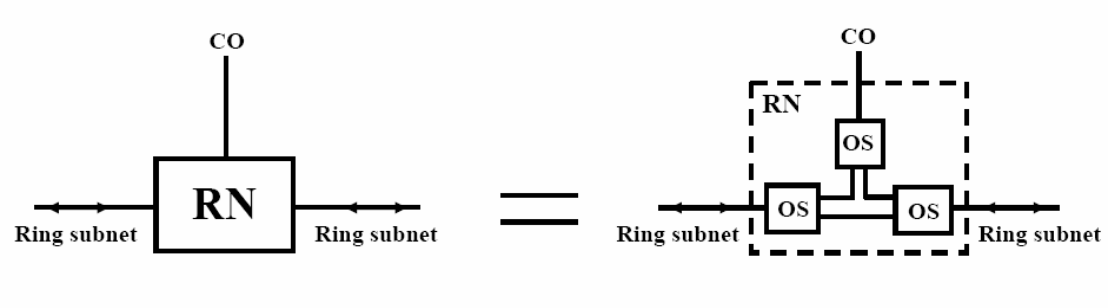

Fig. 3.16 Schematic diagram of remote node (OS: 1x2 optical switch).

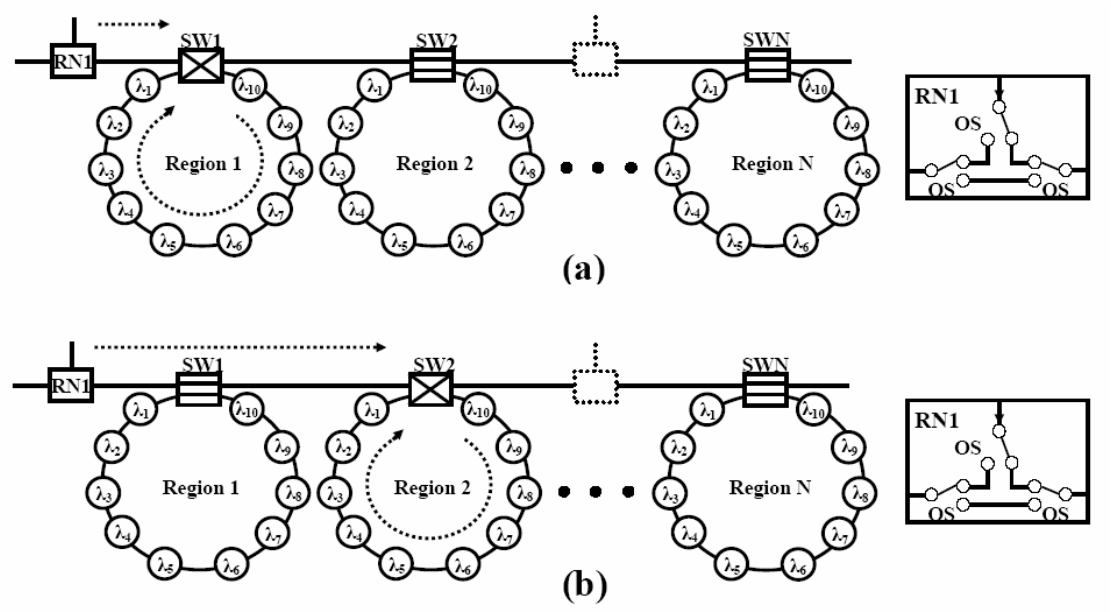

Fig. 3.17 Schematic situation (indicated by dashed line)

(a) when Sensing Region 1 is selected using TDM signal.

(b) when Sensing Region 2 is selected using TDM signal.

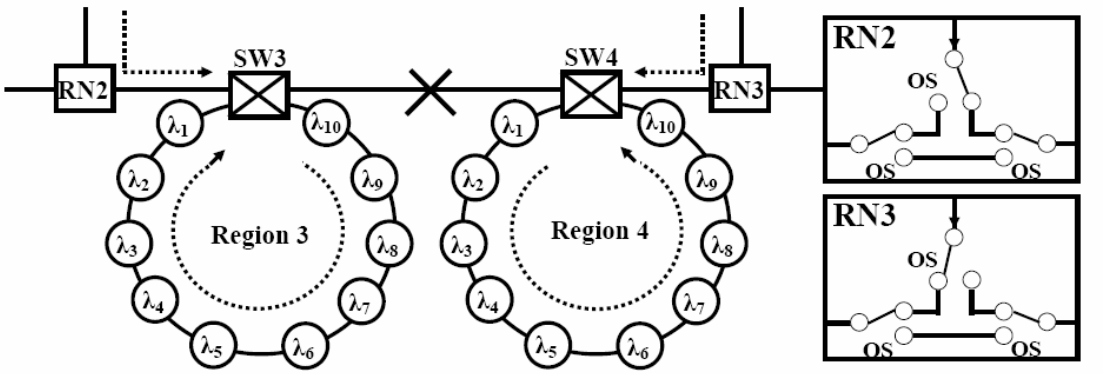

Fig. 3.18 Schematic diagram when breakpoints occur in bus subnet.

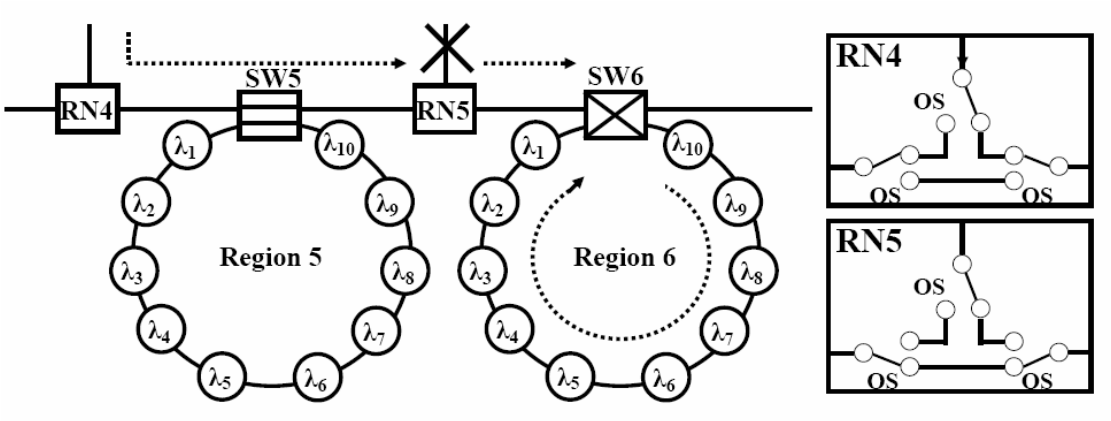

Fig. 3.19 Schematic diagram when breakpoints occur in star subnet.

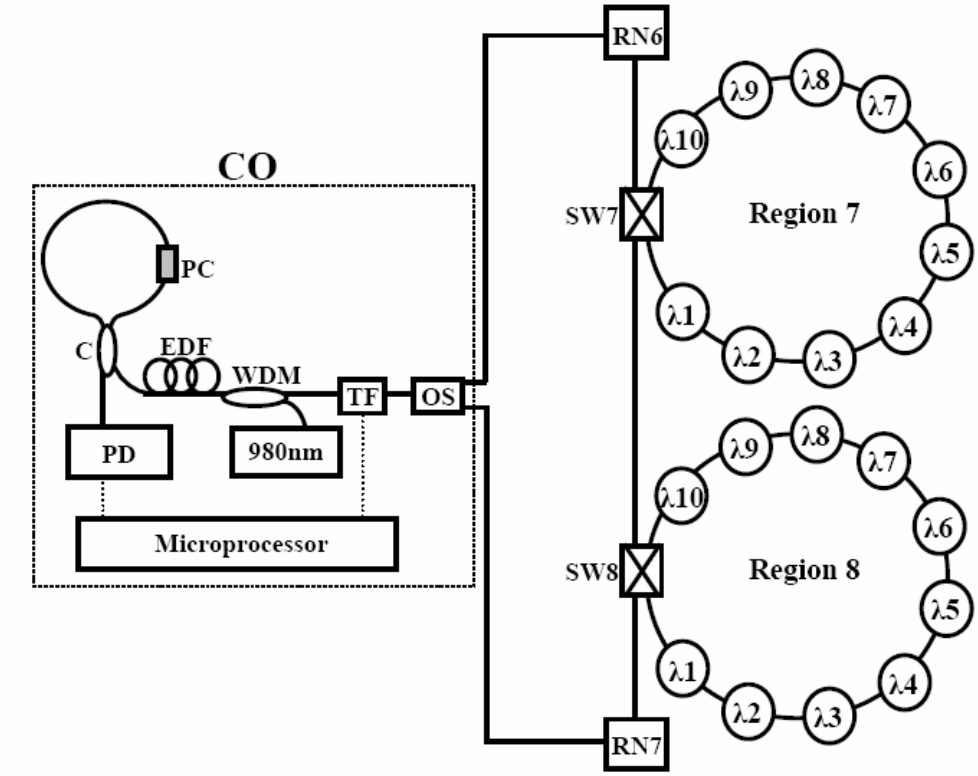

Fig. 3.20 Experimental setup for proposed FBG sensor network. (PC: polarization controller, TF: tunable band-pass filter, EDF: erbium-doped fiber, λm: FBG, C: 2x2 coupler, WDM: 980/1550 nm WDM coupler, PD: photo detector).

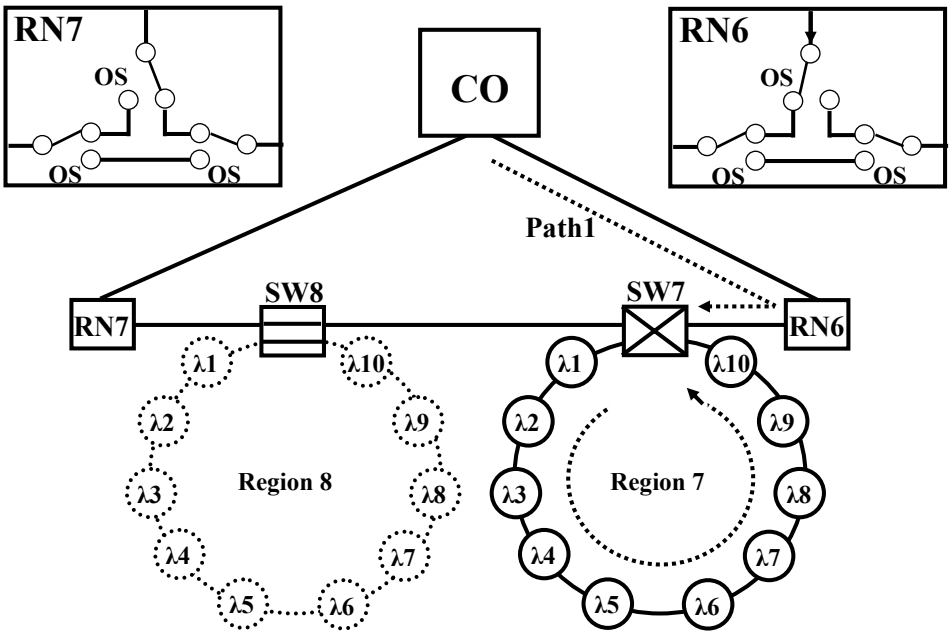

Fig. 3.21 Schematic diagram when Sensing Region 7 is selected.

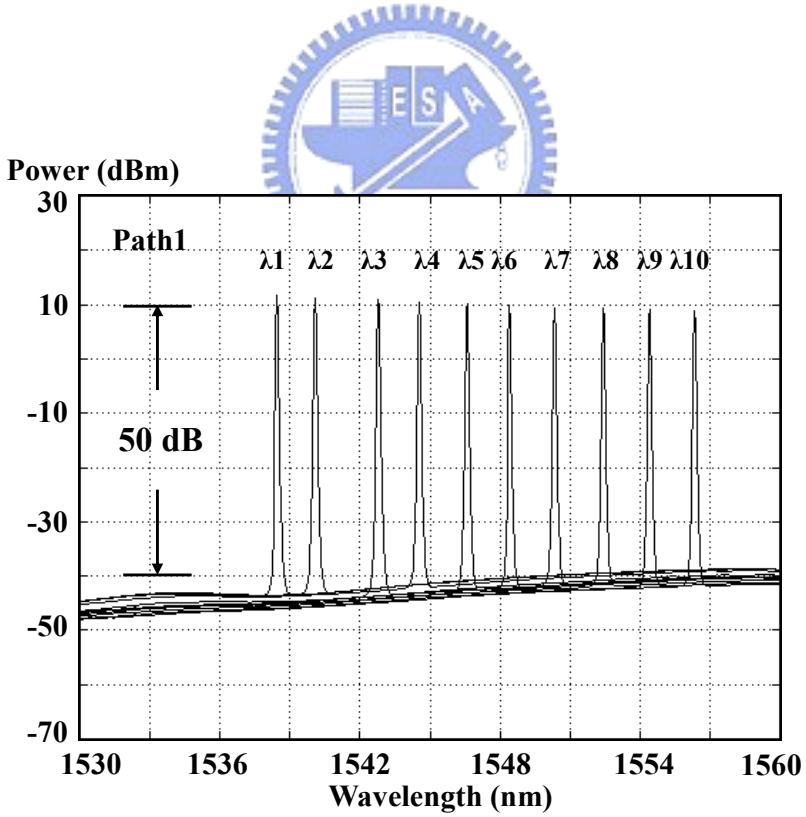

Fig. 3.22 Output spectra of linear-cavity fiber laser at different lasing wavelengths.

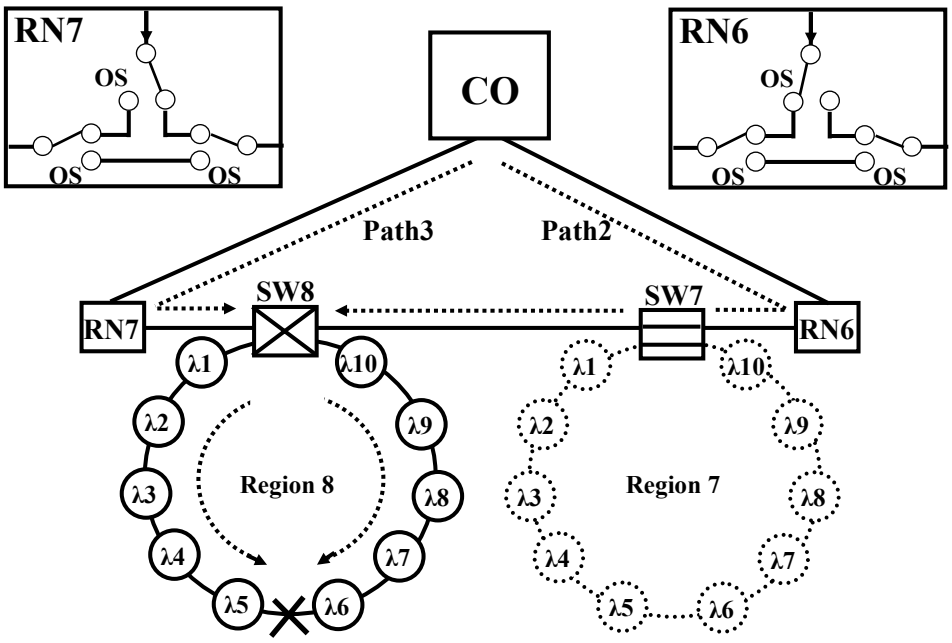

Fig. 3.23 Schematic diagram when Sensing Region 8 is selected.

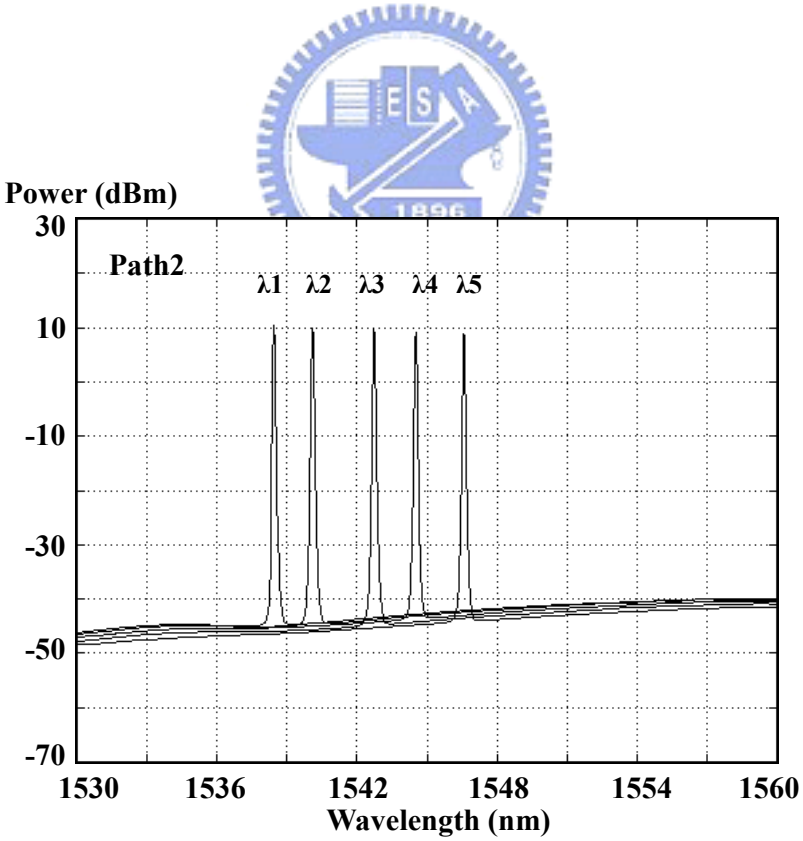

Fig. 3.24 When link fails, sensing information FBG λm (m=6, 7, 8, 9, and 10) is lost.

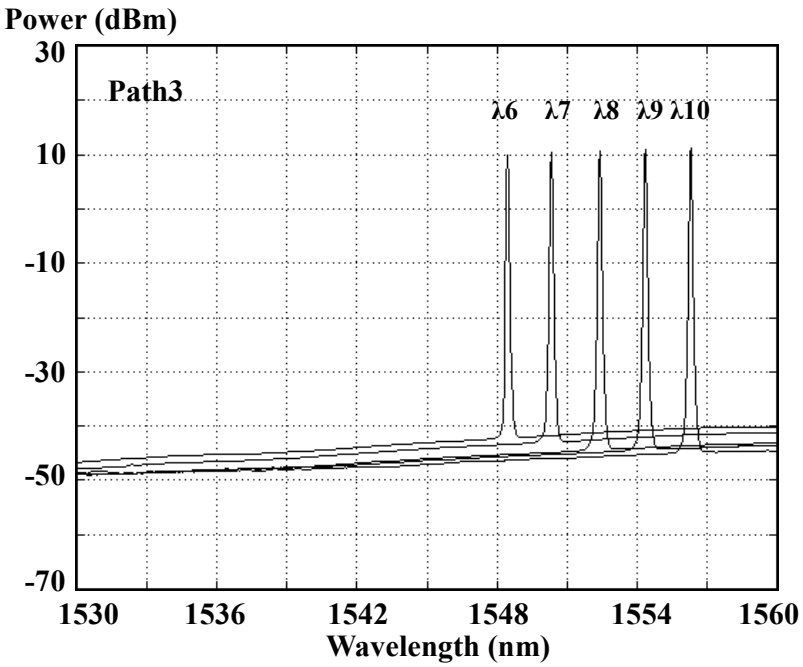

Fig. 3.25 The RN7 is modified to reconfigure the fiber link for FBG λm (m=6, 7, 8, 9, and 10) that lost sensing information.

Architecture	**Ring**	**Star-Ring**	**Star-Bus-Ring**
Cost	Cheap	Medium	Expensive
Reliability	Poor	Good	Medium
Capacity	Medium	Least	Largest

Table 3.1 Brief comparisons of the proposed architectures**.**